J. Appl. Comput. Mech., 11(4) (2025) 1087-1102
DOI: 10.22055/jacm.2025.48044.4937

ISSN: 2383-4536
jacm.scu.ac.ir

Shahid Chamran University of Ahvaz

Journal of Applied and Computational Mechanics

Research Paper

Vibration Characteristics-based Isogeometric Analysis of Sandwich Plates with an Auxetic Honeycomb Core and Laminated Three-phase Skin Layers Resting on Kerr Foundation

Pham Binh Le[1], Chung Pham[2], Truong Thi Huong Huyen[1], Nguyen Manh Dung[1], Trung Thanh Tran[1]

[1] Faculty of Mechanical Engineering, Le Quy Don Technical University, Hanoi, Vietnam,
Email: lephambinh@lqdtu.edu.vn (P.B.L.); huonghuyen.hvktqs@gmail.com (T.T.H.H.); dr307161996@gmail.com (N.M.D.); tranthanh0212@gmail.com (T.T.T.)

[2] Faculty of Aerospace Engineering, Le Quy Don Technical University, Hanoi, Vietnam, Email: phamchunghk2002@gmail.com

Received November 25 2024; Revised January 03 2025; Accepted for publication January 05 2025.
Corresponding author: T.T. Tran (tranthanh0212@gmail.com)

Abstract. The main goal of this paper is to introduce an isogeometric analysis (IGA) procedure based on Reddy's higher-order shear deformation theory (HSDT) for vibration analysis of sandwich plates resting on Kerr foundation (KF). The sandwich plates include the ultra-light feature of the auxetic honeycomb core layer and are reinforced by two laminated three-phase skin layers. The governing equation is derived from Hamilton's principle. The Newmark-beta method is applied to solve the vibration characteristics of the sandwich plates using the code in Matlab software. The reliability and accuracy of the proposed formula are verified through comparative examples. Additionally, the effects of geometrical dimensions, material properties, boundary conditions (BCs), and foundation stiffness on the vibration of sandwich plates are studied in detail. Our findings indicate that the initial geometry of the auxetic honeycomb core has a significant impact on the vibration characteristics of sandwich plates.

Keywords: Sandwich plates, isogeometric analysis, auxetic honeycomb, Kerr foundation, vibration characteristics.

1. Introduction

Recent advances in additive manufacturing (AM) have revolutionized the design and production of complex bio-inspired engineering structures, of which negative Poisson's ratio honeycomb structures (specifically auxetic honeycomb structures) are no exception. Early studies on honeycomb structures yielding negative Poisson's ratio and its advantages were introduced by Wan et al. [1] and Zhang et al. [2]. Then, Zhu et al. [3] using Galerkin solution to study the nonlinear vibration of honeycomb sandwich plates. Cong et al. [4] modified a third-order exact solution to analyze the dynamic behavior of sandwich shells. Duc et al. [5, 6] shown effects of geometrical parameters, material properties on vibration of honeycomb sandwich plates by using an exact solution. Due to the use of analytical methods, the above studies are limited to complex models and arbitrary boundary conditions (BCs). Tran et al. [7] examined forced vibration of honeycomb sandwich plates based on first-order finite element formulation. Overall, the above studies show some positive effects of honeycomb structure on the mechanical behavior of the structures, and indicate its suitability as the core of sandwich structures to reduce the overall mass.

Several investigations have confirmed the effectiveness of sandwich constructions with foam or honeycomb cores. For example, Nguyen et al. [8], Eipakchi et al. [9, 10], and Pham et al. [11]. Besides, Nouraei et al. [12] analyzed the vibration of sandwich plates with an auxetic core using numerical and analytical solution methods. Aktas [3] studied the wave propagation behavior in sandwich composite nanoplates with a metamaterial honeycomb core layer and double FG ultra-stiff surface layers based on an exact solution. Sobhy and Al Mukahal [14] examined wave propagation in sandwich structures with a honeycomb core layer employing a closed-form solution. In addition, Studies on nanometer-sized sandwich structures can be found in the available literature [15, 16]. Honeycomb constructions provide better shear and impact resistance as well as improved energy absorption capacities when compared to standard foam structures. Consequently, honeycomb material shows up as a good option for sandwich architectures' middle layer [17]. On the contrary, three-phase polymer/graphene nanoplatelets (GNP)/fiber structures, which are renowned for their exceptional strength, become prominent candidates for the outer coating layers of sandwich structures. Several authors have introduced different methods in combination with varying plate theories to analyze the response of three-phase polymer/GNP/fiber structures including Cheng et al. [18], Swain et al. [19], Saeedi et al. [20], Yousefi et al. [21, 22], Noroozi et al. [23]. Moreover, Jeawon et al. [24] utilized a Sequential Quadratic Programming solution to optimize the frequency of three-phase polymer/GNP plates. The results from the above studies demonstrate the durability of the three-phase polymer/GNP/fiber structure and its perfect suitability as the skin of a sandwich structure.

Published online: January 17 2025

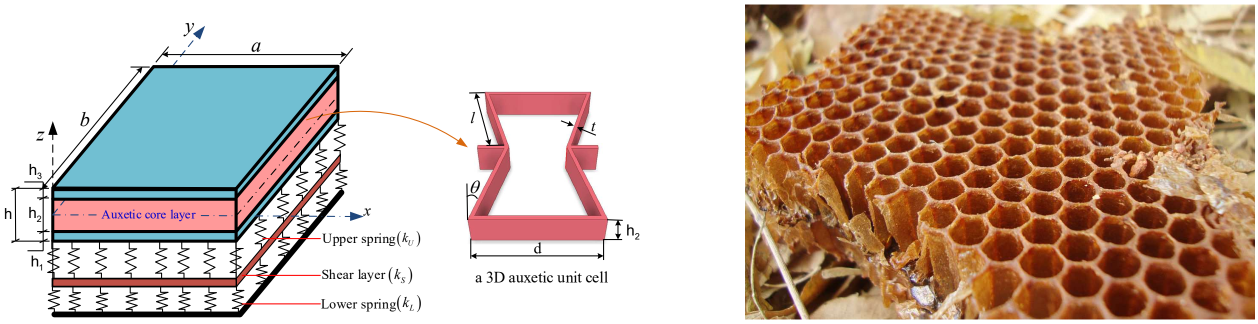

(a) (b)

Fig. 1. Problem model in Cartesian coordinate system and geometrical dimensions, (a) The sandwich plate model resting on KF, (b) Honeycomb nest in nature (source: internet).

Nowadays, with the development of computer technology, FEM and meshless methods can solve many engineering problems with different levels of complexity, however, for structures with complex geometry, the problem of meshing or dividing points can become a problem. To overcome this problem, the isogeometric method (IGA) has been a topic attracting much research in recent years. The isogeometric method is a numerical method proposed by Hughes et al. [25, 26], which is a combination of Computer-Aided Design (CAD) geometric modeling and finite element analysis. This combination is expressed in the use of the same shape functions in the geometric and finite element models, so instead of using basic shape functions based on Lagrange polynomials, IGA uses basic shape functions in the geometric model (B-splines). The IGA approach approximates field variables based on control points instead of element nodes, which speeds up convergence, improves accuracy, and reduces computation time. Some work on FG structural analysis using IGA can be found in the literature [27-35]. Recently, with the explosion of artificial intelligence (AI) and big data. Structural analysis based on the combination of traditional methods and artificial neural networks (ANN); deep neural networks (DNN); and machine learning (ML) [36-39] has attracted the attention of scientists worldwide. The advantage of this method is that it can control uncertain input parameters and accurately predict possible results based on previously available data sources [40, 41], which greatly reduces the computational time and cost. This can be regarded as a new advance in structural analysis.

It can be observed that IGA is a modern numerical method, most suitable for analyzing the mechanical behavior of structures. The extension of IGA based on different plate theories has been carried out by many authors. With that goal in mind, in this study, we introduce a new IGA procedure based on Reddy's simple polynomial high-order shear theory to analyze the free and forced vibrations of sandwich plates with an auxetic honeycomb core and laminated three-phase skin layers supported by KF. The accuracy of the proposed method is verified through comparative examples. In addition, the effect of geometrical dimensions, material properties, BCs, and foundation stiffness on the vibration of sandwich plates is examined in detail.

2. Model Problem

2.1. The auxetic honeycomb core

Considering the sandwich plate with parameters as presented in Fig. 1(a). A group of $h_1 - h_2 - h_3$ denotes the skin-core-skin layer thickness ratio of the sandwich plate (so-called configuration). The auxetic honeycomb structures inspired by natural biology (Fig. 1(b)) are increasingly used in many potential fields, such as civil construction, automotive, aerospace, defence, etc., due to their high strength, excellent vibration absorption, and lightweight. Some assumptions about the sandwich plate model are given as follows:

- The material components work within the elastic limit;
- The material properties are deterministic parameters, ignoring random (uncertain) factors;
- The sandwich plate does not delaminate and separate from the elastic base during vibration;
- The sandwich plates used are of moderate thickness and thin.

The mechanical properties of the honeycomb core are defined as follows [3, 8]:

$$\begin{gathered}
E_1^c = E_0 \frac{\lambda_3^3(\lambda_1 - \sin\theta)}{\cos\theta[\cos^2\theta + \lambda_3^2(\lambda_1 + \sin^2\theta)]};\, E_2^c = E_0 \frac{\lambda_3^3(\lambda_1 - \sin\theta)}{\cos\theta(\lambda_1 - \sin\theta)(\tan^2\theta + \lambda_3^2)}; \\
G_{12}^c = E_0 \frac{\lambda_3^3}{\lambda_1(1+2\lambda_1)\cos\theta};\, G_{13}^c = G_0 \frac{\lambda_3^3}{2\cos\theta}\left[\frac{\lambda_1 - \sin\theta}{1+2\lambda_1} + \frac{\lambda_1 + 2\sin^2\theta}{2(\lambda_1 - \sin\theta)}\right];\, G_{23}^c = G_0 \frac{\lambda_3 \cos\theta}{\lambda_1 - \sin\theta}; \\
\rho^c = \rho_0 \frac{\lambda_3(\lambda_1 + 2)}{2\cos\theta(\lambda_1 - \sin\theta)};\, \upsilon_{12}^c = \frac{-\sin\theta(\lambda_1 - \sin\theta)(1-\lambda_3^2)}{[\cos^2\theta + \lambda_3^2(\lambda_1 + \sin^2\theta)]};\, \upsilon_{21}^c = \frac{-\sin\theta(1-\lambda_3^2)}{(\tan^2\theta + \lambda_3^2)(\lambda_1 - \sin\theta)}
\end{gathered} \tag{1}$$

where $\lambda_1 = d/l$ and $\lambda_3 = t/l$. The effect of θ and λ_1 on Poisson's ratio with $\lambda_3 = 0.1$ is shown in Fig. 2. Observing that θ gets values from $0°$ to $80°$, Poisson's ratio is negative.

2.2. The three-phase skin layer

2.2.1. The GNP-reinforced polymer

According to the rule of mixture, the Poisson's ratio υ_{Gm} and the density ρ_{Gm} of the GNP are gained $(V_m + V_{GNP} = 1)$ as follows:

$$\upsilon_{Gm} = \upsilon_m V_m + \upsilon_{GNP} V_{GNP} \tag{2a}$$

$$\rho_{Gm} = \rho_m V_m + \rho_{GNP} V_{GNP} \tag{2b}$$

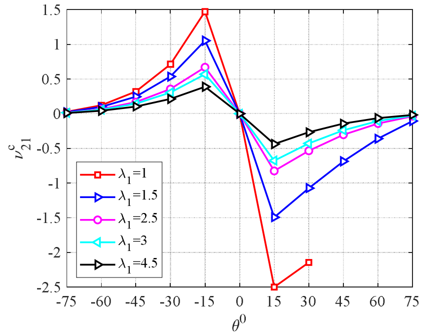

Fig. 2. The Poisson's ratio versus θ with different values of λ_1 [16].

The GNP volume fraction is calculated through the weight fraction W_{GNP} as follows [42]:

$$V_{GNP} = \frac{\rho_m W_{GNP}}{\rho_m + \rho_{GNP}(1 - W_{GNP})} \tag{3}$$

The GNP-reinforced polymer's elastic modulus is obtained by using the Halpin-Tsai model as follows [43]:

$$E_{Gm} = \left(\frac{5}{8}\left(\frac{1 + \xi_W \eta_W V_{GNP}}{1 - \eta_W V_{GNP}} \right) + \frac{3}{8}\left(\frac{1 + \xi_L \eta_L V_{GNP}}{1 - \eta_L V_{GNP}} \right) \right) E_m \tag{4a}$$

in which

$$\xi_W = \frac{2W_{GNP}}{h_{GNP}};\ \xi_W = \frac{2l_{GNP}}{h_{GNP}};\ \eta_W = \frac{\eta - 1}{\eta + \xi_W};\ \eta_L = \frac{\eta - 1}{\eta + \xi_L};\ \eta = \frac{E_{GNP}}{E_m};\ G_{Gm} = \frac{E_{Gm}}{2(1 + \upsilon_{Gm})} \tag{4b}$$

with W_{GNP}, l_{GNP}, and h_{GNP} denote the width, length, and thickness of the GNPs, respectively.

2.2.2. The three-phase skin layers

A three-phase polymer/GNP/fiber density following the rule of the mixture as $(V_{Gm} + V_F = 1)$:

$$\rho_f = \rho_F V_F + \rho_{Gm} V_{Gm} \tag{5}$$

with the fibers volume fraction is defined following weight fraction (W_F) by [42]:

$$V_F = \frac{\rho_{Gm} W_F}{\rho_{Gm} + \rho_F (1 - W_F)} \tag{6}$$

For the three-phase skin layers, the elastic moduli (E^f_{ij}), shear moduli (G^f_{ij}), and Poisson's ratio (υ^f_{ij}) as obtained by:

$$\begin{gathered}
E^f_{11} = E^F_{11} V_F + E^F_{Gm} V_{Gm};\ E^f_{22} = \left(\frac{E^F_{22} + E_{Gm} + (E^F_{22} - E_{Gm})V_F}{E^F_{22} + E_{Gm} - (E^F_{22} - E_{Gm})V_F} \right) E_{Gm}; \\
G^f_{12} = G^f_{13} = \frac{G^F_{22} + G_{Gm} + (G^F_{22} - G_{Gm})V_F}{E^F_{22} + E_{Gm} - (G^F_{22} - G_{Gm})V_F} G_{Gm};\ G^f_{23} = \frac{E^f_{22}}{2(1 + \upsilon^f_{23})}; \\
\upsilon^f_{12} = \upsilon^F_{12} V_F + \upsilon_{Gm} V_{Gm};\ \upsilon^f_{21} = \frac{E^f_{22}}{E^f_{11}} \upsilon^f_{12};\ \upsilon^f_{23} = \upsilon^F_{12} V_F + \upsilon_{Gm} V_{Gm} \left(\frac{1 + \upsilon_{Gm} + \upsilon^f_{12} \frac{E_{Gm}}{E^f_{11}}}{1 + \upsilon^2_{Gm} + \upsilon^f_{12} \upsilon_{Gm} \frac{E_{Gm}}{E^f_{11}}} \right)
\end{gathered} \tag{7}$$

Herein, symbols GNP, m, Gm, f and F represent the GNPs, polymeric matrix, GNP-reinforced matrix, skin layers, and fibers, respectively.

2.3. Kerr foundation

KF consists of an upper layer k_U, a shear layer k_S and a lower layer k_L are defined by [44]:

$$\Re = \frac{k_L k_U}{k_L + k_U} w(x, y) - \frac{k_S k_U}{k_S + k_U} \left[\left(\frac{\partial w}{\partial x} \right)^2 + \left(\frac{\partial w}{\partial y} \right)^2 \right] \tag{8}$$

The KF degenerates into Pasternak foundation (PF) when k_U gets infinity [39]:

$$\Re = k_L w(x, y) - k_s \left[\left(\frac{\partial w}{\partial x} \right)^2 + \left(\frac{\partial w}{\partial y} \right)^2 \right] \tag{9}$$

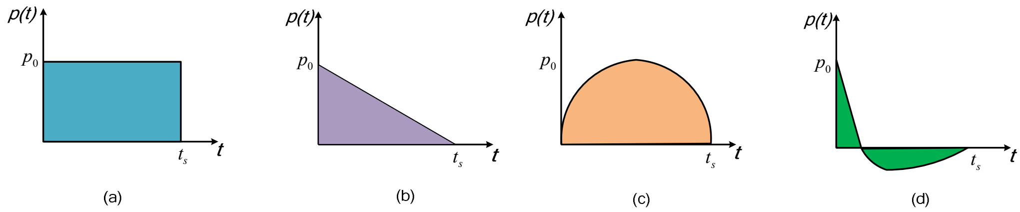

Fig. 3. Pressure vs. time graph of different types of impulse loads [45], (a) Step load, (b) Triangular load, (c) Sinusoidal load, (d) Blast load.

2.4. Pulse loads

As shown in Fig. 3, the excitations in this paper consist of four different types of pulse loads, which are expressed as follows [45]:

- Step loading:

$$p(t)=\begin{cases}P_0 & 0\le t\le t_s\\ 0 & t\ge t_s\end{cases} \tag{10a}$$

- Triangular loading:

$$p(t)=\begin{cases}P_0\left(1-\dfrac{t}{t_s}\right) & 0\le t\le t_s\\ 0 & t\ge t_s\end{cases} \tag{10b}$$

- Sinusoidal loading:

$$p(t)=\begin{cases}P_0\sin\left(\dfrac{\pi t}{t_s}\right) & 0\le t\le t_s\\ 0 & t\ge t_s\end{cases} \tag{10c}$$

- Blast loading:

$$p(t)=\begin{cases}P_0\left(1-\dfrac{t}{t_s}\right)e^{-\gamma t/t_s} & 0\le t\le t_s\\ 0 & t\ge t_s\end{cases} \tag{10d}$$

in which P_0 represents the peak value of different pulse loads, t_s represents the duration of the load, and γ represents the attenuation coefficient of blast load.

3. Basis Formulation

3.1. The displacement field

Following Reddy's HSDT, the displacement field is determined by [46]:

$$\begin{cases}u(x,y,z)=u_0(x,y)-z\theta_x-\dfrac{4}{3h^2}z^3(\theta_x+w_{,x})\\ v(x,y,z)=v_0(x,y)-z\theta_y-\dfrac{4}{3h^2}z^3(\theta_y+w_{,y})\\ w(x,y,z)=w_0(x,y)\end{cases} \tag{11}$$

where u_0, v_0, w_0 are middle-surface displacements; θ_x and θ_y are rotations of the normal in xz and yz planes, respectively.

The strain-displacement relations as:

$$\varepsilon=\varepsilon_m+z\kappa_1+z^3\kappa_2 \tag{12a}$$

$$\gamma=\varepsilon_s+z^2\kappa_s \tag{12b}$$

in which ε_m is the membrane strain, κ_1,κ_2 are bending strains, and γ is the transverse shear strain as:

$$\varepsilon_m=\begin{Bmatrix}u_{0,x}\\ v_{0,y}\\ u_{0,y}+v_{0,x}\end{Bmatrix};\kappa_1=\begin{Bmatrix}\theta_{x,x}\\ \theta_{y,y}\\ \theta_{x,y}+\theta_{y,x}\end{Bmatrix};\kappa_2=\begin{Bmatrix}\theta_{x,x}+w_{x,x}\\ \theta_{y,y}+w_{y,y}\\ \theta_{x,y}+\theta_{y,x}+2w_{x,y}\end{Bmatrix}; \tag{13a}$$

$$\varepsilon_s=\begin{Bmatrix}\theta_x+w_{,x}\\ \theta_y+w_{,y}\end{Bmatrix};\kappa_s=3c\begin{Bmatrix}\theta_x+w_{,x}\\ \theta_y+w_{,y}\end{Bmatrix} \tag{13b}$$

The stress-strain relation following Hooke's law is:

$$\begin{Bmatrix}\sigma_x\\ \sigma_y\\ \tau_{xy}\\ \tau_{xz}\\ \tau_{yz}\end{Bmatrix}=\begin{bmatrix}Q_{11} & Q_{12} & 0 & 0 & 0\\ Q_{21} & Q_{22} & 0 & 0 & 0\\ 0 & 0 & Q_{66} & 0 & 0\\ 0 & 0 & 0 & Q_{55} & Q_{45}\\ 0 & 0 & 0 & Q_{45} & Q_{44}\end{bmatrix}\begin{Bmatrix}\varepsilon_x\\ \varepsilon_y\\ \gamma_{xy}\\ \gamma_{xz}\\ \gamma_{yz}\end{Bmatrix} \tag{14}$$

where, for the auxetic honeycomb core, one has [46]:

$$Q_{11}^c=\frac{E_1^c}{1-\upsilon_{12}^c\upsilon_{21}^c};Q_{22}^c=\frac{E_2^c}{1-\upsilon_{12}^c\upsilon_{21}^c};Q_{12}^c=Q_{21}^c=\frac{\upsilon_{12}^c E_1^c}{1-\upsilon_{12}^c\upsilon_{21}^c};Q_{44}^c=G_{23}^c;Q_{55}^c=G_{13}^c;Q_{66}^c=G_{12}^c;Q_{45}^c=0 \tag{15}$$

and for the three-phase skin layers [47]:

$$\begin{bmatrix}Q_{11}^s & Q_{12}^s & Q_{16}^s & 0 & 0\\ Q_{12}^s & Q_{22}^s & Q_{26}^s & 0 & 0\\ Q_{16}^s & Q_{26}^s & Q_{66}^s & 0 & 0\\ 0 & 0 & 0 & Q_{55}^s & Q_{45}^s\\ 0 & 0 & 0 & Q_{45}^s & Q_{44}^s\end{bmatrix}=\begin{bmatrix}m^2 & m^2 & -2mn & 0 & 0\\ m^2 & m^2 & 2mn & 0 & 0\\ mn & -mn & m^2-n^2 & 0 & 0\\ 0 & 0 & 0 & m & -n\\ 0 & 0 & 0 & n & m\end{bmatrix}\begin{bmatrix}\bar{Q}_{11}^s & \bar{Q}_{12}^s & 0 & 0 & 0\\ \bar{Q}_{12}^s & \bar{Q}_{22}^s & 0 & 0 & 0\\ 0 & 0 & \bar{Q}_{66}^s & 0 & 0\\ 0 & 0 & 0 & \bar{Q}_{55}^s & 0\\ 0 & 0 & 0 & 0 & \bar{Q}_{44}^s\end{bmatrix}\begin{bmatrix}m^2 & m^2 & -2mn & 0 & 0\\ m^2 & m^2 & 2mn & 0 & 0\\ mn & -mn & m^2-n^2 & 0 & 0\\ 0 & 0 & 0 & m & -n\\ 0 & 0 & 0 & n & m\end{bmatrix} \tag{16}$$

where $m=\cos(\varphi_k)$ and $n=\sin(\varphi_k)$ in which φ_k denotes the fiber angle in the k^{th} layer, and:

$$\bar{Q}_{11}^s=\frac{E_1^f}{1-\upsilon_{12}^f\upsilon_{21}^f};\bar{Q}_{22}^s=\frac{E_2^f}{1-\upsilon_{12}^f\upsilon_{21}^f};Q_{12}^s=\upsilon_{12}^f\bar{Q}_{22}^s;\bar{Q}_{44}^s=G_{23}^f;\bar{Q}_{55}^s=G_{13}^f;\bar{Q}_{66}^s=G_{12}^f \tag{17}$$

The stress resultants are computed by:

$$\begin{Bmatrix}\mathbb{N}\\ \mathbf{M}\\ \wp\end{Bmatrix}=\mathbb{C}_1\begin{Bmatrix}\varepsilon_m\\ \kappa_1\\ \kappa_2\end{Bmatrix};\begin{Bmatrix}\mathbb{Q}\\ \mathbb{R}\end{Bmatrix}=\mathbb{C}_2\begin{Bmatrix}\varepsilon_s\\ \kappa_s\end{Bmatrix} \tag{18}$$

where,

$$\mathbb{C}_1=\begin{bmatrix}\mathbf{A} & \mathbf{B} & \mathbf{B}^b\\ \mathbf{B} & \mathbf{F} & \mathbf{F}^b\\ \mathbf{B}^b & \mathbf{F}^b & \mathbf{H}\end{bmatrix};\ \mathbb{C}_2=\begin{bmatrix}\mathbf{A}^s & \mathbf{B}^s\\ \mathbf{B}^s & \mathbf{F}^s\end{bmatrix} \tag{19}$$

in there, $\mathbf{A},\mathbf{B},\mathbf{F},\mathbf{B}^b,\mathbf{F}^b,\mathbf{H},\mathbf{A}^s,\mathbf{B}^s$ and $\mathbf{F}^s$ are the material elastic matrices determined by:

$$(\mathbf{A},\mathbf{B},\mathbf{F},\mathbf{B}^b,\mathbf{F}^b,\mathbf{H})=\int_{-h/2}^{h/2}\begin{bmatrix}Q_{11} & Q_{12} & 0\\ Q_{21} & Q_{22} & 0\\ 0 & 0 & Q_{66}\end{bmatrix}(1,z,z^2,z^3,z^4,z^6)dz; \tag{20a}$$

$$(\mathbf{A}^s,\mathbf{B}^s,\mathbf{F}^s)=\int_{-h/2}^{h/2}(1,z^2,z^4)\begin{bmatrix}Q_{55} & Q_{45}\\ Q_{45} & Q_{44}\end{bmatrix}dz \tag{20b}$$

Replacing Eq. (19) into Eq. (18), we get:

$$\begin{Bmatrix}\mathbb{N}\\ \mathbf{M}\\ \wp\\ \mathbb{Q}\\ \mathbb{R}\end{Bmatrix}=\begin{bmatrix}\mathbf{A} & \mathbf{B} & \mathbf{B}^b & \mathbf{0} & \mathbf{0}\\ \mathbf{B} & \mathbf{F} & \mathbf{F}^b & \mathbf{0} & \mathbf{0}\\ \mathbf{B}^b & \mathbf{F}^b & \mathbf{H} & \mathbf{0} & \mathbf{0}\\ \mathbf{0} & \mathbf{0} & \mathbf{0} & \mathbf{A}^s & \mathbf{B}^s\\ \mathbf{0} & \mathbf{0} & \mathbf{0} & \mathbf{B}^s & \mathbf{F}^s\end{bmatrix}\begin{Bmatrix}\varepsilon_m\\ \kappa_1\\ \kappa_2\\ \varepsilon_s\\ \kappa_s\end{Bmatrix} \tag{21}$$

3.2. The governing equations

The governing equation of the plate following Hamilton's principle is determined by [46]:

$$\int_0^T(\delta U+\delta U^f+\delta W-\delta T)\,dt=0 \tag{22}$$

in which, the virtual strain energy is defined by:

$$\delta U=\int_\Omega\left[(\delta\varepsilon_m)^T\mathbb{N}+(\delta\kappa_1)^T\mathbf{M}+(\delta\kappa_2)^T\wp+(\delta\varepsilon_s)^T\mathbb{Q}+(\delta\kappa_s)^T\mathbb{R}\right]d\Omega \tag{23}$$

The virtual work done by external forces is determined as follows:

$$\delta W=-\int_\Omega q(t)\delta w d\Omega \tag{24}$$

The virtual deformed foundation is represented by:

$$\delta U^{f}=\int_{\Omega}\Re\delta w d\Omega \tag{25}$$

The virtual kinetic energy is calculated by:

$$\delta T=\int_{\Omega}(\delta\dot{\mathbf{u}}_1^T\chi\,\dot{\mathbf{u}}_1+\delta\dot{\mathbf{u}}_2^T\chi\,\dot{\mathbf{u}}_2+\delta\dot{\mathbf{u}}_3^T\chi\,\dot{\mathbf{u}}_3)\,dxdy=\int_{\Omega}\delta\dot{\mathbf{u}}^T\Upsilon\ddot{\mathbf{u}}\,d\Omega \tag{26}$$

with Υ is the matrix of inertial components, defined by:

$$\Upsilon=\begin{bmatrix}\chi & 0 & 0\\ 0 & \chi & 0\\ 0 & 0 & \chi\end{bmatrix} \tag{27}$$

where

$$\chi=\begin{bmatrix}l_0 & l_1 & l_3\\ l_1 & l_2 & l_4\\ l_3 & l_4 & l_6\end{bmatrix} \tag{28}$$

with

$$(l_0,l_1,l_2,l_3,l_4,l_6)=\int_{-h/2}^{h/2}\rho(z)(1,z,z^2,z^3,z^4,z^6)\,dz \tag{29}$$

The displacement vectors are expressed by:

$$\mathbf{u}=\begin{Bmatrix}\mathbf{u}_1\\ \mathbf{u}_2\\ \mathbf{u}_3\end{Bmatrix};\mathbf{u}_1=\begin{Bmatrix}u_0\\ -w_{,x}\\ \theta_x\end{Bmatrix};\mathbf{u}_2=\begin{Bmatrix}v_0\\ -w_{,y}\\ \theta_y\end{Bmatrix};\mathbf{u}_3=\begin{Bmatrix}w\\ 0\\ 0\end{Bmatrix};\ \dot{\mathbf{u}}_1=\begin{Bmatrix}\dot{u}_0\\ -\dot{w}_{,x}\\ \dot{\theta}_x\end{Bmatrix};\dot{\mathbf{u}}_2=\begin{Bmatrix}\dot{v}_0\\ -\dot{w}_{,y}\\ \dot{\theta}_y\end{Bmatrix};\dot{\mathbf{u}}_3=\begin{Bmatrix}\dot{w}\\ 0\\ 0\end{Bmatrix} \tag{30}$$

The weak form of the plate is determined by [46]:

$$\int_{\Omega}\left[(\delta\varepsilon)^T\mathbb{C}_1\varepsilon+(\delta\gamma)^T\mathbb{C}_2\gamma\right]d\Omega+\int_{\Omega}\mathbf{R}(\delta w)\,d\Omega+\int_{\Omega}\delta\mathbf{u}^T\Upsilon\ddot{\mathbf{u}}\,d\Omega=\int_{\Omega}q(t)(\delta w)d\Omega \tag{31}$$

3.3. Isogeometric analysis procedure

The displacement field is approximated by the NURBS functions by [25]:

$$\mathbf{u}(\xi,\eta)=\sum_{K=1}^{p\times q}\mathbf{R}_K(\xi,\eta)\mathbf{d}_K \tag{32}$$

where $\mathbf{d}_K=\{u_{0K},v_{0K},w_K,\theta_{xK},\theta_{yK}\}^T$ represents the displacement of control point K, and $\mathbf{R}_K$ denotes the shape function [26]. Substituting Eq. (32) into Eq. (13), we get:

$$[\varepsilon_m;\ \kappa_1;\ \kappa_2;\ \varepsilon_s;\ \kappa_s]=\sum_{K=1}^{p\times q}[\mathbf{B}_m;\ \mathbf{B}_1;\ \mathbf{B}_2;\ \mathbf{B}_{s1};\ \mathbf{B}_{s2}]\mathbf{d}_K \tag{33}$$

in which

$$\mathbf{B}_m=\begin{bmatrix}\mathbf{R}_{K,x} & 0 & 0 & 0 & 0\\ 0 & \mathbf{R}_{K,y} & 0 & 0 & 0\\ \mathbf{R}_{K,y} & \mathbf{R}_{K,x} & 0 & 0 & 0\end{bmatrix} \tag{34a}$$

$$\mathbf{B}_1=\begin{bmatrix}0 & 0 & 0 & \mathbf{R}_{K,x} & 0\\ 0 & 0 & 0 & 0 & \mathbf{R}_{K,y}\\ 0 & 0 & 0 & \mathbf{R}_{K,y} & \mathbf{R}_{K,x}\end{bmatrix} \tag{34b}$$

$$\mathbf{B}_2=c\begin{bmatrix}0 & 0 & \mathbf{R}_{K,xx} & \mathbf{R}_{K,x} & 0\\ 0 & 0 & \mathbf{R}_{K,yy} & 0 & \mathbf{R}_{K,y}\\ 0 & 0 & 2\mathbf{R}_{K,xy} & \mathbf{R}_{K,y} & \mathbf{R}_{K,x}\end{bmatrix} \tag{34c}$$

$$\mathbf{B}_{s1}=\begin{bmatrix}0 & 0 & \mathbf{R}_{K,x} & \mathbf{R}_K & 0\\ 0 & 0 & \mathbf{R}_{K,y} & 0 & \mathbf{R}_K\end{bmatrix} \tag{34d}$$

$$\mathbf{B}_{s2}=\begin{bmatrix}0 & 0 & \mathbf{R}_{K,x} & \mathbf{R}_K & 0\\ 0 & 0 & \mathbf{R}_{K,y} & 0 & \mathbf{R}_K\end{bmatrix} \tag{34e}$$

Substituting Eq. (30) into Eq. (28), the motion equation of plates is determined by:

$$\mathbf{M}\ddot{\mathbf{d}} + (\mathbf{K} + \mathbf{K}_f)\mathbf{d} = \mathbf{F} \tag{35}$$

where, the plate stiffness matrix is:

$$\mathbf{K} = \int_{\Omega} \left(\begin{bmatrix} \mathbf{B}_m \\ \mathbf{B}_1 \\ \mathbf{B}_2 \end{bmatrix}^T \begin{bmatrix} \mathbf{A} & \mathbf{B} & \mathbf{B}^b \\ \mathbf{B} & \mathbf{F} & \mathbf{F}^b \\ \mathbf{B}^b & \mathbf{F}^b & \mathbf{H} \end{bmatrix} \begin{bmatrix} \mathbf{B}_m \\ \mathbf{B}_1 \\ \mathbf{B}_2 \end{bmatrix}^T + \begin{bmatrix} \mathbf{B}_{s1} \\ \mathbf{B}_{s2} \end{bmatrix}^T \begin{bmatrix} \mathbf{A}^s & \mathbf{B}^s \\ \mathbf{B}^s & \mathbf{F}^s \end{bmatrix} \begin{bmatrix} \mathbf{B}_{s1} \\ \mathbf{B}_{s2} \end{bmatrix} \right) \tag{36}$$

The plate mass matrix is:

$$\mathbf{M} = \int_{\Omega} \begin{bmatrix} \mathbf{H}_1 \\ \mathbf{H}_2 \\ \mathbf{H}_3 \end{bmatrix} \begin{bmatrix} \chi & 0 & 0 \\ 0 & \chi & 0 \\ 0 & 0 & \chi \end{bmatrix} \begin{bmatrix} \mathbf{H}_1 \\ \mathbf{H}_2 \\ \mathbf{H}_3 \end{bmatrix} d\Omega \tag{37}$$

where

$$\mathbf{H}_1 = \begin{bmatrix} \mathbf{R}_K & 0 & 0 & 0 & 0 \\ 0 & 0 & \mathbf{R}_{K,x} & 0 & 0 \\ 0 & 0 & 0 & \mathbf{R}_K & 0 \end{bmatrix} \tag{38a}$$

$$\mathbf{H}_2 = \begin{bmatrix} 0 & \mathbf{R}_K & 0 & 0 & 0 \\ 0 & 0 & \mathbf{R}_{K,y} & 0 & 0 \\ 0 & 0 & 0 & 0 & \mathbf{R}_K \end{bmatrix} \tag{38b}$$

$$\mathbf{H}_3 = \begin{bmatrix} 0 & 0 & \mathbf{R}_K & 0 & 0 \\ 0 & 0 & 0 & 0 & 0 \\ 0 & 0 & 0 & 0 & 0 \end{bmatrix} \tag{38c}$$

The foundation stiffness matrix is:

$$\mathbf{K}^f = \frac{k_L k_U}{k_L + k_U} \int_{\Omega} (\mathbf{R}_K)^T \mathbf{R}_K d\Omega + \frac{k_S k_U}{k_S + k_U} \int_{\Omega} [(\mathbf{R}_{K,x})^T (\mathbf{R}_{K,x}) + (\mathbf{R}_{K,y})^T (\mathbf{R}_{K,y})] d\Omega \tag{39}$$

The transverse load vector as:

$$\mathbf{F} = \int_{\Omega} q(t)\mathbf{R} d\Omega \tag{40}$$

Now, the motion equation of the plate is:

$$\mathbf{M}\ddot{\mathbf{q}} + (\mathbf{K} + \mathbf{K}_f)\mathbf{q} = \mathbf{F} \tag{41}$$

Taking into account the structural damping, Eq. (41) is rewritten by:

$$\mathbf{M}\ddot{\mathbf{q}} + \mathbf{C}\dot{\mathbf{q}} + (\mathbf{K} + \mathbf{K}_f)\mathbf{q} = \mathbf{F} \tag{42}$$

in which $\mathbf{C} = \alpha\mathbf{M} + \beta\mathbf{K}$, with α and β are Rayleigh damping factors defined through damping ratio ζ and the first two natural frequencies as [47]:

$$\beta = \frac{2\zeta}{\omega_1 + \omega_2};\ \alpha = \frac{2\omega_1\omega_2\zeta}{\omega_1 + \omega_2} \tag{43}$$

To solve Eq. (42), the Newmark method is used with steps as shown in [48]. In this article, Dirichlet boundary is applied with displacement constraints on the edges of plates (Fig. 4) as follows:

- Clamped (C): $u_0 = v_0 = w = \theta_x = \theta_y = 0$ at all edges;
- Simply supported (S): $u_0 = w = \theta_x = 0$ at $y = 0, y = b$ and/or $v_0 = w = \theta_y = 0$ at $x = 0, x = a$;
- Free (F): all edges are not supported.

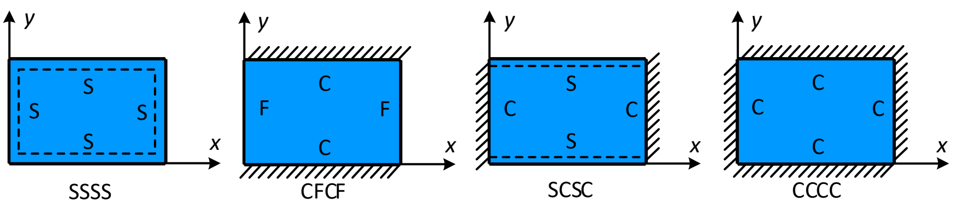

Fig. 4. The types of BCs.

Table 1. The adopted material properties.

Materials	Young's modulus E (GPa)	Density ρ (kg/m³)	Poisson's ratio υ
Al [44]	70	2707	0.3
Al_2O_3 [44]	380	3800	0.3
Epoxy [24]	3	1200	0.34
GNPs [24]	1010	1060	0.186

Table 2. Comparison of dimensionless frequencies of SSSS FG square sandwich plates (h = a/10).

n	Frequencies	Methods						
		Present	[8]	Er (%)	[49]	Er (%)	[50]	Er (%)
1	ω_1^*	1.2997	1.3049	0.40	1.3019	0.17	1.3001	0.03
	ω_2^*	3.1417	3.1640	0.70	3.1606	0.60	3.1492	0.24
	ω_3^*	3.1417	3.1645	0.72	3.1606	0.60	3.1492	0.24
	ω_4^*	4.8666	4.8896	0.47	4.9188	1.06	4.8941	0.56
	ω_5^*	5.9572	5.9507	0.11	6.0586	1.67	6.0094	0.87
10	ω_1^*	0.9441	0.9461	0.21	0.9418	0.24	0.9430	0.12
	ω_2^*	2.2995	2.3160	0.71	2.2948	0.20	2.3003	0.03
	ω_3^*	2.2995	2.3164	0.73	2.2948	0.20	2.3003	0.03
	ω_4^*	3.5869	3.6247	1.04	3.5832	0.10	3.5969	0.28
	ω_5^*	4.4114	4.4235	0.27	4.4225	0.25	4.4330	0.49

Note: $\mathrm{Er}(\%) = 100 \times \left|\omega_{pr}^* - \omega_{re}^*\right| / \left|\omega_{re}^*\right|$; where ω_{pr}^* and ω_{re}^* are dimensionless frequencies of our work and previous studies, respectively.

Table 3. Comparison of dimensionless frequencies of SSSS FG square plates (a/h=10).

Frequencies	Power-law index (n)									
	Ceramic		0.5		1		5		Metal	
	Present	[51]	Present	[51]	Present	[51]	Present	[51]	Present	[51]
$\bar{\omega}_1$	0.05765	0.05767	0.04894	0.04816	0.04409	0.04448	0.03757	0.03782	0.02931	0.02933
$\bar{\omega}_2$	0.13704	0.13764	0.11675	0.11633	0.10518	0.10748	0.0883	0.09	0.06969	0.06999
$\bar{\omega}_3$	0.13704	0.13764	0.11675	0.11633	0.10518	0.10748	0.0883	0.09	0.06969	0.06999
$\bar{\omega}_4$	0.19483	0.19476	0.17478	0.17033	0.16102	0.16184	0.12623	0.1261	0.09908	0.09904
$\bar{\omega}_5$	0.19483	0.19476	0.17478	0.17033	0.1619	0.16184	0.12623	0.1261	0.09908	0.09904
$\bar{\omega}_6$	0.20913	0.2112	0.17873	0.18017	0.1619	0.16651	0.1335	0.13767	0.10635	0.1074
$\bar{\omega}_7$	0.25371	0.25753	0.21725	0.2208	0.19574	0.20413	0.16111	0.16751	0.12902	0.13096
$\bar{\omega}_8$	0.25371	0.25753	0.21725	0.2208	0.19574	0.20413	0.16111	0.16751	0.12902	0.13096
$\bar{\omega}_9$	0.27554	0.27543	0.24711	0.24081	0.22879	0.22871	0.17824	0.17804	0.14011	0.14006
$\bar{\omega}_{10}$	0.31593	0.32298	0.27123	0.27868	0.24441	0.25773	0.19925	0.20942	0.16066	0.16424

4. Numerical Results

Within the scope of the study, geometric dimensions and material properties are assumed to be deterministic parameters, ignoring random (uncertain) factors. The value ranges of the input parameters are determined by referring to previously published studies. The constituent material properties are shown in Table 1.

4.1. Verification

Firstly, considering a fully simply supported (SSSS) FG (Al/Al_2O_3) square sandwich plate (2-1-2) with a pure ceramic core and n is power-law index. The dimensionless natural frequency is given by the formula $\omega^* = (\omega a^2 / h)\sqrt{\rho_0 / E_0}$ with $E_0 = 1\,GPa$ and $\rho_0 = 1\,kg/m^3$. The first five dimensionless frequencies of sandwich plates in comparison with those of IGA-based polygon elements [8], QUAD-8 using HSDT (Q8-HSDT) [49], and IGA-TSDT [50] are presented in Table 2. It can be confirmed that the gained results of the current method match well with those of other published (maximum error of approximately 1%).

Secondly, to further verify the accuracy of the proposed method, the obtained dimensionless frequencies $\bar{\omega}_i = \omega_i h\sqrt{\rho_{Al_2O_3} / E_{Al_2O_3}}$ of the FG (Al/Al_2O_3) square plate are compared with those of Vasiraja et al. [51] using Shell181 element with a mesh size of 50x50 in ANSYS®15.0 software. These results are presented in Tables 3 and 4 for the two cases of SSS and CCCC FG plates, respectively. It can be seen that our results are close to those of ANSYS®15.0 software implemented by Vasiraja et al. [51].

Thirdly, the SSSS FG (Al/Al_2O_3) square plate with $h = a/20$ resting on Pasternak foundation is studied. The dimensionless parameters are provided by $K_L = k_1 a^4 / H_b$, $K_S = k_2 a^2 / H_b$, with $H_b = E_{Al} h^3 / [12(1-\upsilon_{Al}^2)]$; $\Omega = \omega h\sqrt{\rho_{Al} / E_{Al}}$. The results are robustly correlated with those derived from a closed-form solution employing a novel hyperbolic quasi-3D theory [52] and TSDT [53], as listed in Table 5.

Table 4. Comparison of dimensionless frequencies of CCCC FG square plates (a/h=10).

Frequencies	Power-law index (n)									
	Ceramic		0.5		1		5		Metal	
	Present	[51]	Present	[51]	Present	[51]	Present	[51]	Present	[51]
$\overline{\omega}_1$	0.0988	0.0984	0.08441	0.08274	0.07619	0.07656	0.06365	0.06362	0.05024	0.05004
$\overline{\omega}_2$	0.18829	0.18779	0.16162	0.15983	0.14593	0.14803	0.11977	0.12061	0.09575	0.09549
$\overline{\omega}_3$	0.18829	0.18779	0.16162	0.15983	0.14593	0.14803	0.11977	0.12061	0.09575	0.09549
$\overline{\omega}_4$	0.26306	0.26318	0.22649	0.22584	0.20451	0.20928	0.16596	0.16849	0.13377	0.13383
$\overline{\omega}_5$	0.30895	0.3103	0.26657	0.26759	0.24075	0.24807	0.19386	0.19793	0.1571	0.15779
$\overline{\omega}_6$	0.31137	0.31327	0.26865	0.26986	0.24265	0.2502	0.19553	0.19982	0.15834	0.1593
$\overline{\omega}_7$	0.37134	0.37271	0.32099	0.32476	0.28991	0.3014	0.23175	0.23855	0.18883	0.18953
$\overline{\omega}_8$	0.37134	0.37271	0.32099	0.32476	0.28991	0.3014	0.23175	0.23855	0.18883	0.18953
$\overline{\omega}_9$	0.37269	0.37517	0.33414	0.32607	0.30916	0.30923	0.24064	0.24076	0.18952	0.19078
$\overline{\omega}_{10}$	0.37269	0.37517	0.33414	0.32607	0.30916	0.30923	0.24064	0.24076	0.18952	0.19078

Table 5. The dimensionless fundamental frequencies of FG square plates resting on PF.

(K_L, K_S), $K_U=\infty$	n	The frequency Ω		
		Proposed method	Quasi-3D [52]	TSDT [53]
(0, 0)	0	0.0291	0.0290	0.0291
	1	0.0222	0.0227	0.0226
	2	0.0202	0.0209	0.0206
	5	0.0191	0.0197	0.0195
(100, 0)	0	0.0298	0.0298	0.0298
	1	0.0233	0.0238	0.0236
	2	0.0214	0.0221	0.0218
	5	0.0204	0.0210	0.0208
(100, 100)	0	0.0411	0.0411	0.0411
	1	0.0384	0.0388	0.0386
	2	0.0380	0.0386	0.0383
	5	0.0383	0.0388	0.0385

Finally, the deflection response of the SSSS FG (Al/Al_2O_3) square plate with dimension $a=b=0.2\ m, h=0.025\ m$, under a step load $q_0(x,y)=50\ MPa$ is plotted in Fig. 5. It can be seen that the gained deflection response is a good similarity both in shape and value with those of Abuteir et al. [54] using a degenerated shell element. The above examples have verified the performance and reliability of the proposed formula. Note that, in this paper, a mesh size of 13x13 is used.

4.2. Free vibration analysis

This section studies the sandwich plate with an auxetic honeycomb core and laminated three-phase polymer/GNP/fiber skin layers. The remaining structural parameters include: the dimensions of the GNPs: $l_{GNP}=2.5\mu m$, $w_{GNP}=2.5\mu m$, $h_{GNP}=1.5nm$ with weight fraction of the GNPs: $W_{GNP}=0.01$ [55]; each face sheet consists of four layers of $\varphi=[90^0/45^0/45^0/90^0]$ with the glass fibers' mechanical properties: $E_{11}^F=E_{22}^F=73.084GPa$, $G_{12}^F=30.13GPa$, $\upsilon_{12}^F=0.22$, $\rho_F=2491.191kG/m^3$, and $W_F=0.85$ [49]; the auxetic honeycomb core is made of aluminium (Al). The dimensionless parameters are provided by:

$$K_L=\frac{k_L a^4}{H_{Al}};K_U=\frac{k_U a^4}{H_{Al}}K_S=\frac{k_S a^2}{H_{Al}}\ \text{with}\ H_{Al}=\frac{E_{Al}h^3}{12(1-\upsilon_{Al}^2)} \tag{44}$$

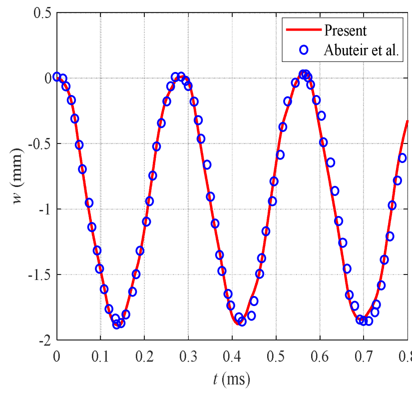

Fig. 5. The time history analysis of SSSS FG square plate center.

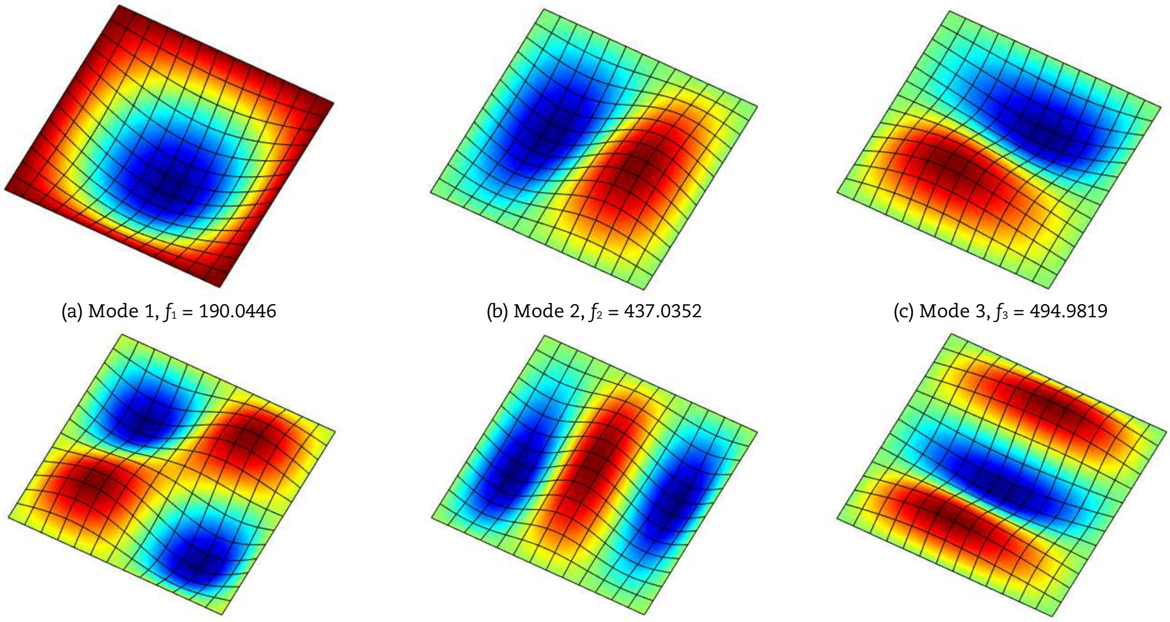

(a) Mode 1, f_1 = 190.0446 (b) Mode 2, f_2 = 437.0352 (c) Mode 3, f_3 = 494.9819

(d) Mode 4, f_4 = 724.6673 (e) Mode 5, f_5 = 841.9280 (f) Mode 6, f_6 = 970.4979

Fig. 6. The eigenmodes of the SSSS square sandwich plate.

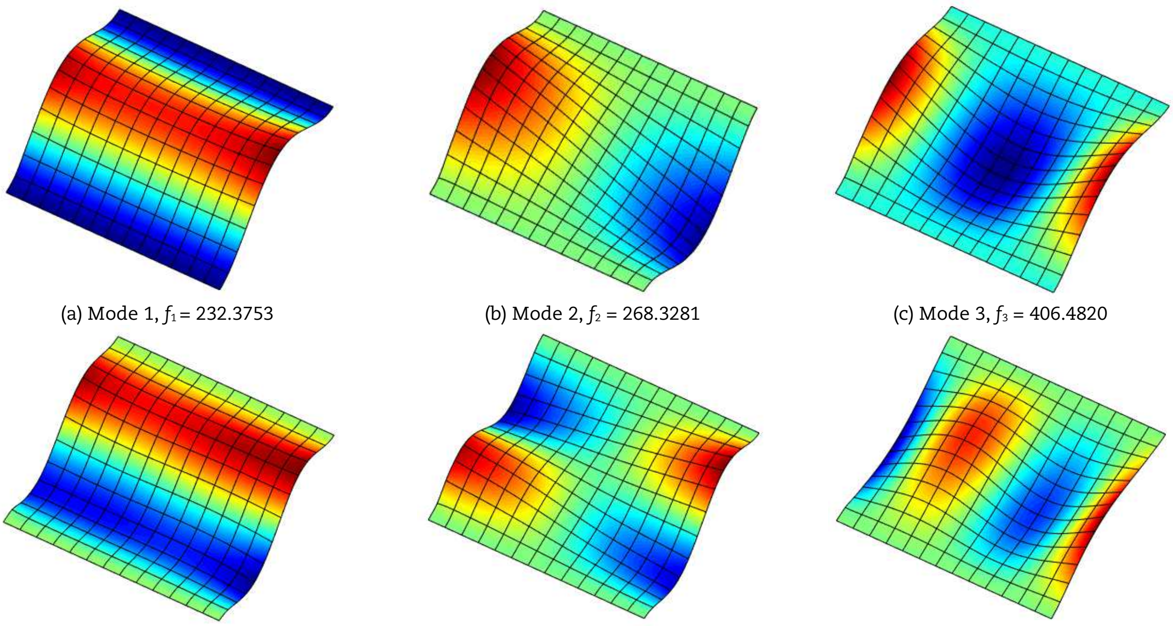

(a) Mode 1, f_1 = 232.3753 (b) Mode 2, f_2 = 268.3281 (c) Mode 3, f_3 = 406.4820

(d) Mode 4, f_4 = 617.2973 (e) Mode 5, f_5 = 666.0608 (f) Mode 6, f_6 = 691.5214

Fig. 7. The eigenmodes of the CFCF square sandwich plate.

Firstly, Fig. 6 shows the first six eigenmodes of the SSSS square sandwich plate (1-1-1) with additional parameters: $h = a/20$, $\lambda_1 = 1.5$, $\lambda_3 = 0.1$, $\theta = 30^0$, $K_L = K_U = 50$, and $K_S = 5$. It can be seen that the second and third eigenmodes are almost identical, differing only in viewing direction due to the square plate being subjected to a simply supported at 4-edge. In addition, Fig. 7 displays the first six eigenmodes of the CFCF square sandwich plate with the above input parameters.

Secondly, Table 6 lists the fundamental frequencies of the square sandwich plate (2-1-2) with $h = a/50$, $K_L = K_U = 25$, and $K_S = 10$ versus values of θ and λ_1 with $\lambda_3 = 0.1$. Observing that the fundamental frequency decreases slightly when θ increases from 10^0 to 40^0, and decreases faster as θ greater than 40^0. Moreover, with each value of θ, an increase of λ_1 increases the frequencies of plates. Besides, the CCCC sandwich plates lead to the maximum fundamental frequencies, as expected. In this study, the value of λ_3 is chosen not greater than 0.2 to ensure the auxetic honeycomb core is light but not easily fragile and vulnerable.

Thirdly, the effect of foundation stiffness on the free vibration of square sandwich plates is displayed in Fig. 8. Specifically, Fig. 8(a) shows the simultaneous effects of the lower spring stiffness K_L and the upper spring stiffness K_U; Fig. 8(b) shows the simultaneous effects of the lower spring stiffness K_L and the shear stiffness K_S; while Fig. 8c shows the mutual interaction of the upper spring stiffness K_U and the shear stiffness K_S on the fundamental frequency of plates. Observing that the foundation stiffness layers increase the sandwich plate stiffness, leading to an increase in the fundamental frequency, as expected. However, the shear and upper layers show a more positive effect on the frequency of sandwich plates. This finding indicates that, if the frequency is to be increased, it is necessary to focus on improving the stiffness of the shear and upper layers.

Table 6. The fundamental frequencies (Hz) of sandwich plates versus θ and λ_1.

θ	The fundamental frequency (Hz)							
	SSSS				CCCC			
	$\lambda_1=1$	$\lambda_1=1.5$	$\lambda_1=2.5$	$\lambda_1=4.5$	$\lambda_1=1$	$\lambda_1=1.5$	$\lambda_1=2.5$	$\lambda_1=4.5$
10^0	71.4176	71.4555	71.4825	71.4991	130.5331	130.6017	130.6505	130.6804
20^0	71.3740	71.4354	71.4729	71.4939	130.4544	130.5654	130.6333	130.6711
30^0	71.2962	71.4044	71.4586	71.4858	130.3133	130.509	130.6073	130.6565
40^0	71.1457	71.3559	71.4373	71.4736	130.0398	130.4209	130.5685	130.6343
50^0	70.8138	71.2776	71.4044	71.4544	129.4363	130.2784	130.5085	130.5994
60^0	69.9199	71.1425	71.3492	71.4217	127.8099	130.0321	130.4078	130.5398
70^0	66.6147	70.8752	71.2397	71.3555	121.7911	129.5453	130.2084	130.4194
80^0	48.2049	70.1200	70.9180	71.1571	88.1984	128.1698	129.6229	130.0585

Table 7. The effects of ratios a/h and h_1-h_2-h_3 on the fundamental frequency of sandwich plates.

a/h	Thickness ratio	The fundamental frequency (Hz)									
		SCSC					CCCC				
		$\lambda_1=1$	$\lambda_1=1.5$	$\lambda_1=2.5$	$\lambda_1=3.5$	$\lambda_1=4.5$	$\lambda_1=1$	$\lambda_1=1.5$	$\lambda_1=2.5$	$\lambda_1=3.5$	$\lambda_1=4.5$
10	2-1-2	484.81	486.70	487.44	487.66	487.77	600.89	602.99	603.80	604.05	604.17
	1-1-1	516.52	521.71	523.78	524.41	524.72	634.99	640.65	642.89	643.58	643.91
	1-2-1	557.14	569.09	573.97	575.48	576.21	677.74	690.50	695.66	697.24	698.01
	1-4-1	588.45	625.28	641.69	646.96	649.56	704.63	743.58	760.51	765.87	768.50
	1-6-1	595.28	658.21	688.89	699.11	704.23	704.11	770.82	802.20	812.46	817.57
	1-8-1	602.89	677.80	715.78	728.66	735.15	708.72	788.02	826.67	839.50	845.93
50	2-1-2	104.67	105.13	105.31	105.36	105.39	134.41	135.00	135.23	135.30	135.33
	1-1-1	112.47	113.77	114.28	114.44	114.51	143.67	145.32	145.97	146.17	146.26
	1-2-1	122.47	125.53	126.78	127.16	127.34	155.35	159.21	160.78	161.25	161.49
	1-4-1	128.59	137.89	142.04	143.36	144.01	160.29	171.84	176.99	178.62	179.43
	1-6-1	128.40	143.77	151.34	153.85	155.10	157.35	176.16	185.40	188.46	189.99
	1-8-1	129.43	147.52	156.81	159.96	161.54	157.37	179.34	190.60	194.40	196.32
75	2-1-2	69.920	70.229	70.349	70.385	70.403	89.881	90.278	90.432	90.478	90.501
	1-1-1	75.149	76.020	76.363	76.467	76.517	96.110	97.222	97.660	97.793	97.857
	1-2-1	81.857	83.912	84.745	85.000	85.123	103.97	106.57	107.63	107.95	108.11
	1-4-1	85.936	92.173	94.960	95.846	96.282	107.25	115.04	118.52	119.63	120.17
	1-6-1	85.777	96.078	101.16	102.84	103.68	105.23	117.90	124.13	126.20	127.24
	1-8-1	86.451	98.576	104.81	106.92	107.98	105.23	120.02	127.61	130.18	131.47
100	2-1-2	52.478	52.710	52.801	52.828	52.841	67.486	67.784	67.900	67.935	67.952
	1-1-1	56.407	57.062	57.320	57.398	57.436	72.171	73.009	73.339	73.438	73.487
	1-2-1	61.449	62.994	63.620	63.812	63.905	78.083	80.047	80.842	81.085	81.203
	1-4-1	64.508	69.197	71.292	71.958	72.285	80.548	86.413	89.034	89.867	90.276
	1-6-1	64.380	72.122	75.939	77.206	77.838	79.014	88.549	93.245	94.805	95.583
	1-8-1	64.883	73.995	78.679	80.266	81.064	79.004	90.138	95.856	97.793	98.767

Next, the simultaneous impact of a/h and $h_1-h_2-h_3$ ratios on the fundamental frequency of square sandwich plates with $\theta=40^0$, $\lambda_3=0.15$, $K_L=K_U=60$ and $K_S=20$ is reported in Table 7. Generally, thicker sandwich plates are stiffer, leading to higher frequencies. On the other hand, the sandwich plate with a thicker honeycomb core (2-1-2, 1-1-1, 1-2-1, 1-4-1, 1-6-1, and 1-8-1, respectively) result in higher frequencies (except for the sandwich plate (1-4-1) with $\lambda_1=1$), which may be an interesting finding because sandwich plates with thicker honeycomb cores are lighter but have higher frequency. Moreover, Table 8 lists the first six frequencies of sandwich plates (1-6-1) with $a/h=45$, $\lambda_1=2.5$, $\lambda_3=0.2$, $K_L=K_U=75$, and $K_S=25$.

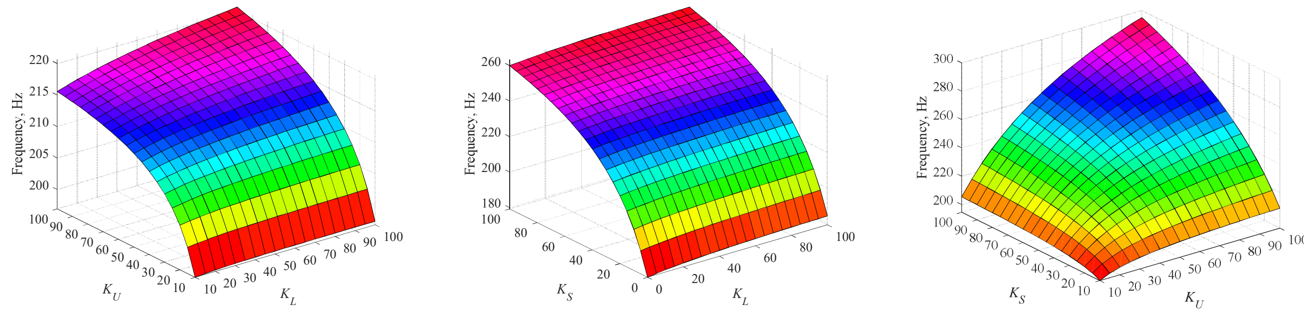

(a) $K_S=15$ (b) $K_U=50$ (c) $K_L=50$

Fig. 8. The effects of foundation stiffness on free vibration of SSSS square sandwich plates (1-4-1) with $h=a/25$, $\theta=20^0$, $\lambda_1=1.5$ and $\lambda_3=0.1$.

Table 8. The first six frequencies of sandwich plates.

BCs	θ	The natural frequency, Hz					
		f_1	f_2	f_3	f_4	f_5	f_6
SSSS	5^0	144.4838	284.4736	312.9172	445.5513	515.39	587.381
	20^0	142.5121	280.596	305.8051	438.935	507.6812	570.1598
	35^0	139.5982	274.8971	300.3517	430.143	497.7644	561.1454
	45^0	136.5586	268.9532	293.9184	420.8833	487.1989	549.2491
	80^0	100.8929	198.9743	217.1736	311.8693	361.3159	405.5236
CFCF	5^0	151.6776	183.9916	281.5403	378.4183	411.3254	452.0776
	20^0	146.8540	179.4159	276.7064	365.1286	398.5288	444.8797
	35^0	144.6438	176.3607	271.3897	360.0038	392.4908	436.2485
	45^0	141.5771	172.5852	265.5302	352.3982	384.1648	426.8967
	80^0	104.2977	127.2512	196.1045	259.4654	283.0831	315.8797
SCSC	5^0	177.8940	330.7594	368.0338	507.6103	601.0080	641.0245
	20^0	175.2384	323.4290	362.4542	499.8494	583.9168	630.7138
	35^0	171.7530	317.6486	355.4033	490.0790	574.5829	618.9698
	45^0	168.0499	310.8751	347.8709	479.6850	562.4333	606.1960
	80^0	124.2797	229.9281	258.0003	356.1825	415.5841	451.5091
CCCC	5^0	216.4768	389.0542	432.2611	582.0069	657.9321	753.8496
	20^0	211.9010	382.3835	420.5119	570.8813	646.9594	730.5086
	35^0	208.0541	375.1447	413.6126	560.3354	635.0016	719.3760
	45^0	203.5999	367.1977	404.8198	548.4654	621.8807	704.1142
	80^0	150.4385	272.2005	298.9057	406.6683	463.0124	519.2359

4.3. Dynamic response analysis

Firstly, the effect of λ_1 on the vibration behavior of SSSS square sandwich plates (1-8-1) subjected to step load is presented in Fig. 9. The input parameters as $a/h = 50$, $\theta = 50^0$, $\lambda_3 = 0.15$, $K_L = K_U = 50$, and $K_S = 15$. It can be concluded that λ_1 has no sensitive effect on the vibration of the plate. However, increasing λ_1 rapidly reduces plate oscillation.

Secondly, the impact of θ on the vibration behavior of SCSC square sandwich plates (1-6-1) subjected to triangular load is presented in Fig. 10. The remaining parameters as $a/h = 60$, $\lambda_1 = 2$, $\lambda_3 = 0.1$, $K_L = K_U = 75$, and $K_S = 25$. It can be seen that the change of θ has little effect on the maximum displacement response of the sandwich plate but affects the speed of oscillation reduction of the sandwich plate.

Thirdly, the influence of K_U on the vibration behavior of CFCF square sandwich plates (2-1-2) subjected to sinusoidal loading is displayed in Fig. 11 with parameters: $a/h = 30$, $\theta = 25^0$, $\lambda_1 = 2$, $\lambda_3 = 0.1$, $K_L = 75$, and $K_S = 25$. As expected, increasing K_U increases the sandwich plate stiffness resulting in a decrease in the displacement and stress response of sandwich plates.

Finally, the effect of thickness ratio on the vibration behavior of CCCC square sandwich plates (1-6-1) subjected to blast load is indicated in Fig. 12. The input parameters as $a/h = 75$, $\theta = 60^0$, $\lambda_1 = 4$, $\lambda_3 = 0.2$, $K_L = K_U = 75$, and $K_S = 45$. It can be found that the thicker the honeycomb core, the larger the range of the trajectory curve, further certifying that the increase of the honeycomb core will increase the vibration velocity of the sandwich plate. The phase curve represents the relationship between the velocity displacement of the plate oscillation with time. It represents the characteristics of the oscillation, in the above studies, the phase curves are smooth and not closed due to the non-periodic oscillation. Note that, the damping ratio $\zeta = 0.1$ and the step interval of the Newmark beta integration method $\Delta t = 6 \times 10^{-5}$s for the above examines.

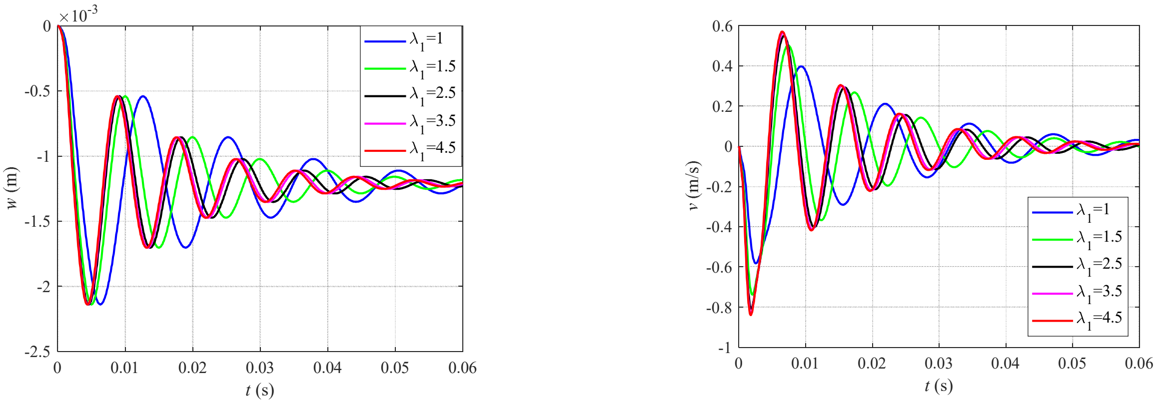

(a) The centre deflection response (b) The centre velocity response

Fig. 9. The effects of λ_1 on the vibration response of SSSS sandwich plates subjected to step load.

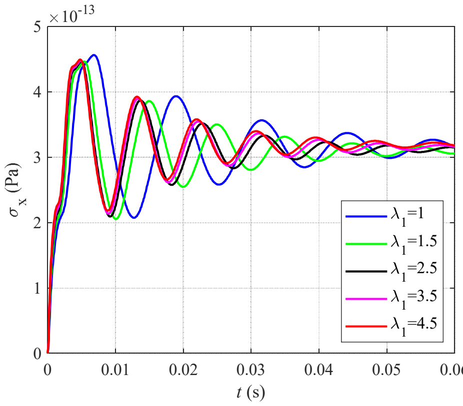

(c) Stress response σ_x (a/2, b/2, 0)

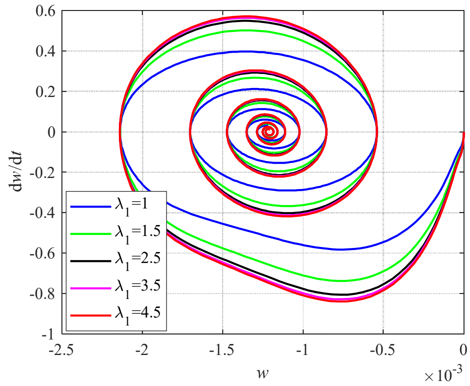

(d) The phase orbit

Fig. 9. Continued.

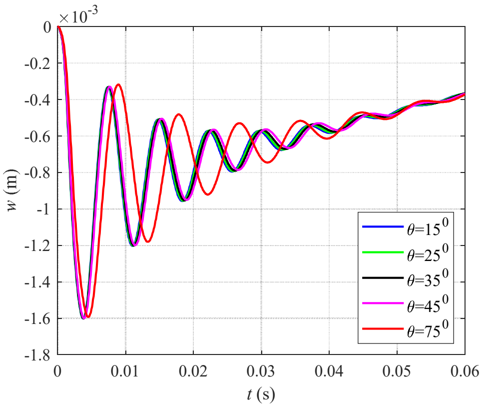

(a) The centre deflection response

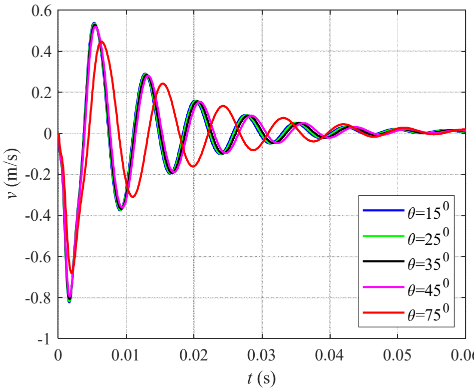

(b) The centre velocity response

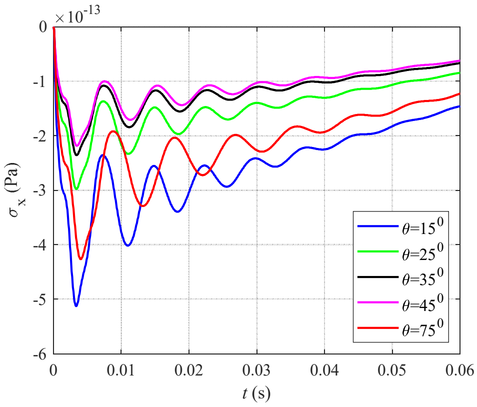

(c) Stress response σ_x (a/2, b/2, 0)

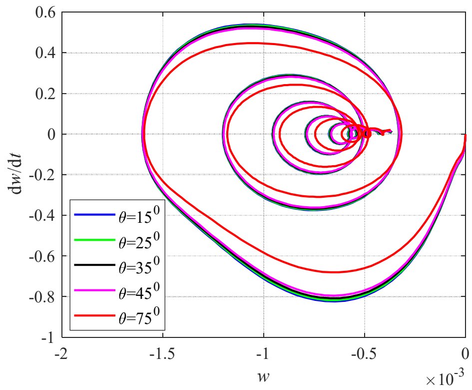

(d) The phase orbit

Fig. 10. The effects of θ on the vibration response of SCSC sandwich plates subjected to triangular load.

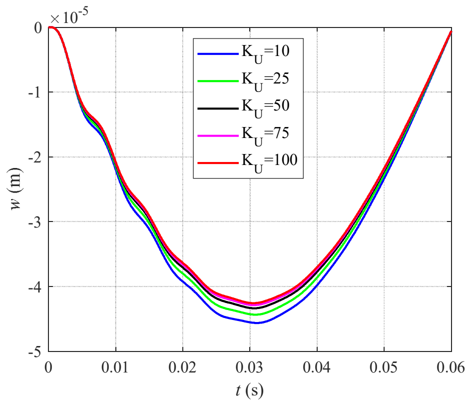

(a) The centre deflection response

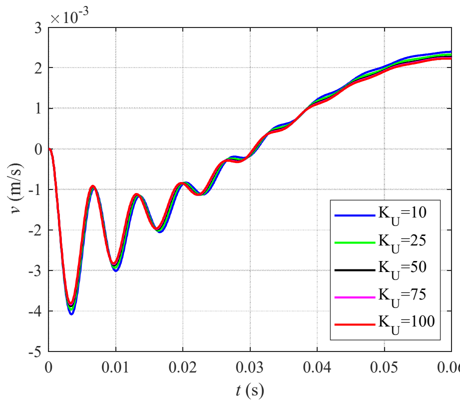

(b) The centre velocity response

Fig. 11. The effects of K_U on the vibration response of CFCF sandwich plates subjected to sinusoidal loading.

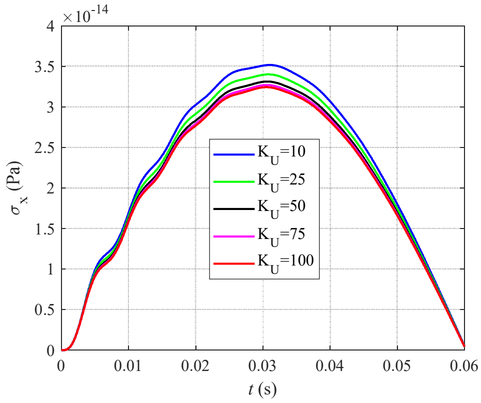

(c) Stress response σ_x (a/2, b/2, 0)

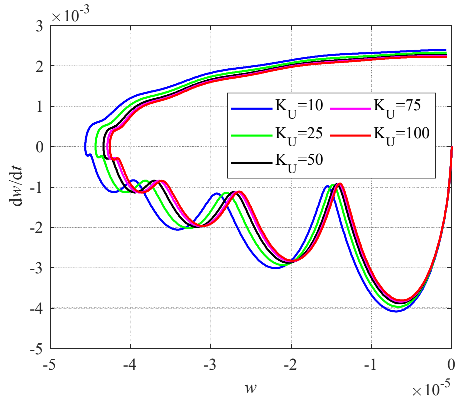

(d) The phase orbit

Fig. 11. Continued.

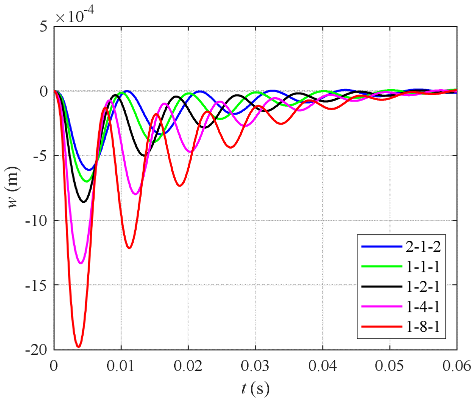

(a) The centre deflection response

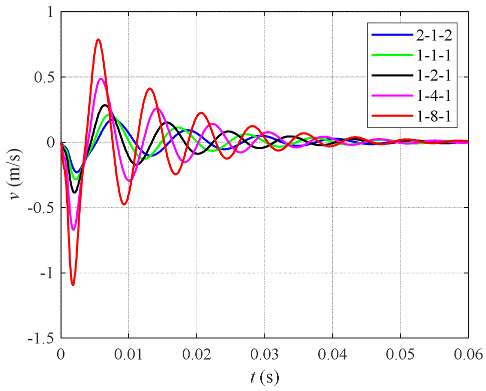

(b) The centre velocity response

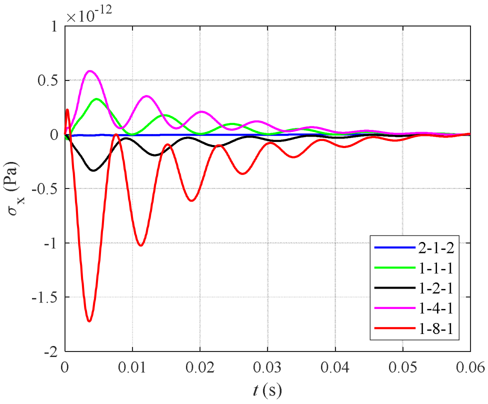

(c) Stress response σ_x (a/2, b/2, 0)

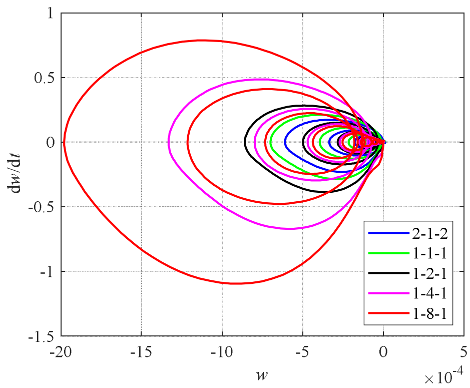

(d) The phase orbit

Fig. 12. The effects of the thickness ratio on the vibration response of CCCC sandwich plates subjected to blast loading.

6. Conclusion

In this work, the authors have successfully developed an isogeometric analysis procedure based on Reddy's HSDT to analyze the vibration behavior of sandwich plates with an auxetic honeycomb core and laminated three-phase skin layers supported by KF subjected to pulse loads. The motion equation of the sandwich plate is derived from Hamilton's principle. Then, the Newmark method is used to solve the vibration response of the sandwich plate. After the above research, the following conclusions can be drawn:

- The increase of λ_1 leads to a decrease in frequency, in the opposite direction the increase of θ reduces the frequency of the sandwich plate. Besides, increasing these two parameters has little effect on the maximum displacement response of the plate but has the effect of making the oscillations damp faster.
- Thicker honeycomb core layers increase the frequency of the sandwich plate but they cause larger plate displacements. In addition, laminated three-phase skin layers help to increase the strength of sandwich plates and protect the honeycomb core subjected to impulse loads, especially blast loads.
- The damping ratio helps to the energy dissipation of the pulse load, the vibration amplitude will decrease and achieve stability faster.
- The elastic foundation helps increase frequency, reduce displacement and stress response of the plate. In which, the upper spring layer and shear layer have much greater impact than the lower spring layer.
- The computational code can be extended to analyze the stability problem and the nonlinear problem with different complex

models. The results are also expected to be useful for practical calculation and design of sandwich plates.
– However, the current method is only applicable when the input parameters are deterministic, analyzing this texture with uncertain input parameters using AI-based algorithms may open up potential research directions in the future.

Author Contributions

The authors have confirmed their contributions to this study as follows: P.B. Le contributed to conceptualization and idea generation. P.B. Le, C. Pham, and T.T. Huong Huyen were responsible for software development and designing computer programs. N.M. Dung and T.T. Thanh assisted in organizing the manuscript and analyzing the results. All authors discussed the results, reviewed, and approved the final version of the manuscript.

Acknowledgments

Not applicable.

Conflict of Interest

The authors declared no potential conflicts of interest concerning the research, authorship, and publication of this article.

Funding

The authors received financial support the Scientific Research Fund of Le Quy Don Technical University Research Found under the grand number “2023.QHT.03” for the research, authorship, and publication of this article.

Data Availability Statements

The datasets generated and/or analyzed during the current study are available from the corresponding author on reasonable request.

References

[1] Wan, H., Ohtaki, H., Kotosaka, S., Hu, G., A study of negative Poisson's ratios in auxetic honeycombs based on a large deflection model, *European Journal of Mechanics-A/Solids*, 23(1), 2024, 95-106.
[2] Zhang, X.C., An, L.Q., Ding, H.M., Zhu, X.Y., El-Rich, M., The influence of cell micro-structure on the in-plane dynamic crushing of honeycombs with negative Poisson’s ratio, *Journal of Sandwich Structures & Materials*, 17(1), 2015, 26-55.
[3] Zhu, X., Zhang, J., Zhang, W., Chen, J., Vibration frequencies and energies of an auxetic honeycomb sandwich plate, *Mechanics of Advanced Materials and Structures*, 26(23), 2019, 1951-1957.
[4] Cong, P.H., Khanh, N.D., Khoa, N.D., Duc, N.D., New approach to investigate nonlinear dynamic response of sandwich auxetic double curves shallow shells using TSDT, *Composite Structures*, 185, 2018, 455-465.
[5] Nguyen, D.D., Pham, C.H., Nonlinear dynamic response and vibration of sandwich composite plates with negative Poisson’s ratio in auxetic honeycombs, *Journal of Sandwich Structures & Materials*, 20(6), 2018, 692-717.
[6] Duc, N.D., Seung, E.K., Cong, P.H., Anh, N.T., Khoa, N.D., Dynamic response and vibration of composite double curved shallow shells with negative Poisson's ratio in auxetic honeycombs core layer on elastic foundations subjected to blast and damping loads, *International Journal of Mechanical Sciences*, 133, 2017, 504-512.
[7] Pham, Q.H., Nguyen, P.C., Tran, T.T., Nguyen-Thoi, T., Free vibration analysis of nanoplates with auxetic honeycomb core using a new third-order finite element method and nonlocal elasticity theory, *Engineering with Computers*, 39, 2023, 233–251.
[8] Nguyen, N.V., Nguyen, X.H., Nguyen, T.N.; Kang, J., Lee, J., A comprehensive analysis of auxetic honeycomb sandwich plates with graphene nanoplatelets reinforcement, *Composite Structures*, 259, 2021, 113213.
[9] Eipakchi, H., Nasrekani, F.M., Vibrational behavior of composite cylindrical shells with auxetic honeycombs core layer subjected to a moving pressure, *Composite Structures*, 254, 2020, 112847.
[10] Eipakchi, H., Nasrekani, F.M., Geometrically nonlinear frequency analysis of composite cylinders with metamaterial honeycomb layer and adjustable Poisson’s ratio using the multiple scale method, *Thin-Walled Structures*, 169, 2021, 10844.
[11] Pham, Q.H., Tran, V.K., Tran, T.T., Vibration characteristics of sandwich plates with an auxetic honeycomb core and laminated three-phase skin layers under blast load, *Defence Technology*, 24, 2023, 148-163.
[12] Nouraei, M., Zamani, V., Civalek, Ö., Vibration of smart sandwich plate with an auxetic core and dual-FG nanocomposite layers integrated with piezoceramic actuators, *Composite Structures*, 315, 2023, 117014.
[13] Aktas, K.G., 3D wave dispersion analysis of graphene platelet-reinforced ultra-stiff double functionally graded nanocomposite sandwich plates with metamaterial honeycomb core layer, *Mechanics of Time-Dependent Materials*, 2024, 1-36.
[14] Sobhy, M., Al Mukahal, F.H., Wave dispersion analysis of functionally graded GPLs-reinforced sandwich piezoelectromagnetic plates with a honeycomb core, *Mathematics*, 10(17), 2022, 3207.
[15] Aktas, K.G., Three-dimensional thermomechanical wave propagation analysis of sandwich nanoplate with graphene-reinforced foam core and magneto-electro-elastic face layers using nonlocal strain gradient elasticity theory, *Acta Mechanica*, 235(9), 2024, 5587-5619.
[16] Pehlivan, F., Esen, I., Aktas, K.G., Thermomechanical Response of Smart Magneto-Electro-Elastic FGM Nanosensor Beams with Intended Porosity, *Arabian Journal for Science and Engineering*, 2024, 1-23.
[17] Pham, Q.H., Nguyen, P.C., Tran, T.T., Free vibration response of auxetic honeycomb sandwich plates using an improved higher-order ES-MITC3 element and artificial neural network, *Thin-Walled Structures*, 175, 2022, 109203.
[18] Cheng, Y., Zhang, K., Liang, B., Cheng, H., Hou, G., Xu, G., Jin, W., Micromechanics of CNT grafted FRP based on hierarchical homogenization of transversely isotropic multi-coated model, *International Journal of Mechanical Sciences*, 161, 2019, 105014.
[19] Swain, A., Roy, T., Viscoelastic modelling and dynamic characteristics of CNTs-CFRP-2DWF composite shell structures, *Composites Part B: Engineering*, 141, 2018, 100-122.
[20] Seidi, J., Kamarian, S., Free vibrations of non-uniform CNT/fiber/polymer nanocomposite beams, *Curved and Layered Structures*, 4(1), 2017, 21-30.
[21] Yousefi, A.H., Memarzadeh, P., Afshari, H., Hosseini, S.J., Agglomeration effects on free vibration characteristics of three-phase CNT/polymer/fiber laminated truncated conical shells, *Thin-Walled Structures*, 157, 2020, 107077.
[22] Yousefi, A.H., Memarzadeh, P., Afshari, H., Hosseini, S.J., Dynamic characteristics of truncated conical panels made of FRPs reinforced with agglomerated CNTs, *Structures*, 33, 2021, 4701-4717.
[23] Noroozi, M., Zajkani, A., Ghadiri, M., Dynamic plastic impact behavior of CNTs/fiber/polymer multiscale laminated composite doubly curved shells, *International Journal of Mechanical Sciences*, 195, 2021, 106223.
[24] Jeawon, Y., Drosopoulos, G., Foutsitzi, G., Stavroulakis, G., Adali, S., Optimization and analysis of frequencies of multi-scale graphene/fibre reinforced nanocomposite laminates with non-uniform distributions of reinforcements, *Engineering Structures*, 228, 2021, 111525.
[25] Hughes, T.J., Cottrell, J.A., Bazilevs, Y., Isogeometric analysis: CAD, finite elements, NURBS, exact geometry and mesh refinement, *Computer Methods*

in Applied Mechanics and Engineering, 194(39-41), 2005, 4135-4195.
[26] Borden, M.J., Scott, M.A., Evans, J.A.; Hughes, T.J., Isogeometric finite element data structures based on Bézier extraction of NURBS, *International Journal for Numerical Methods in Engineering*, 87(1-5), 2011, 15-47.
[27] Nguyen, X.H., Tran, L.V., Thai, C.H., Kulasegaram, S., Bordas, S.P.A., Isogeometric analysis of functionally graded plates using a refined plate theory, *Composites Part B: Engineering*, 64, 2014, 222-234.
[28] Vuong, A.V., Heinrich, C., Simeon, B., ISOGAT: A 2D tutorial MATLAB code for Isogeometric Analysis, *Computer Aided Geometric Design*, 27(8), 2010, 644-655.
[29] Lieu, Q.X., Lee, D., Kang, J., Lee, J., NURBS-based modeling and analysis for free vibration and buckling problems of in-plane bi-directional functionally graded plates, *Mechanics of Advanced Materials and Structures*, 26(12), 2019, 1064-1080.
[30] Phung, V.P., Abdel, W.M., Liew, K., Bordas, S., Nguyen, X.H., Isogeometric analysis of functionally graded carbon nanotube-reinforced composite plates using higher-order shear deformation theory, *Composite Structures*, 123, 2015, 137-149.
[31] Nguyen, V.P., Anitescu, C., Bordas, S.P., Rabczuk, T., Isogeometric analysis: an overview and computer implementation aspects, *Mathematics and Computers in Simulation*, 117, 2015, 89-116.
[32] Echter, R., Bischoff, M., Numerical efficiency, locking and unlocking of NURBS finite elements, *Computer Methods in Applied Mechanics and Engineering*, 199(5-8), 2020, 374-382.
[33] Nguyen, H.X., Nguyen, T.N., Abdel, W.M., Bordas, S.P., Nguyen, X.H., Vo, T.P., A refined quasi-3D isogeometric analysis for functionally graded microplates based on the modified couple stress theory, *Computer Methods in Applied Mechanics and Engineering*, 313, 2017, 904-940.
[34] Natarajan, S., Chakraborty, S., Thangavel, M., Bordas, S., Rabczuk, T., Size-dependent free flexural vibration behavior of functionally graded nanoplates, *Computational Materials Science*, 65, 2012, 74-80.
[35] Anitescu, C., Nguyen, C., Rabczuk, T., Zhuang, X., Isogeometric analysis for explicit elastodynamics using a dual-basis diagonal mass formulation, *Computer Methods in Applied Mechanics and Engineering*, 346, 2019, 574-591.
[36] Zhao, S., Lin, S., Dong, M., Guo, H., Zheng, H., Mass lumping schemes fitted to MLS-based numerical manifold method in vibration of plates with cutouts using CPT and FSDT, *Composite Structures*, 330, 2024, 117815.
[37] Padmanabha, G.A., Fuhg, J.N., Safta, C., Jones, R. E., Bouklas, N., Improving the performance of Stein variational inference through extreme sparsification of physically-constrained neural network models, *Computer Methods in Applied Mechanics and Engineering*, 432, 2024, 117359.
[38] Guo, H., Zhuang, X., Alajlan, N., Rabczuk, T., Physics-informed deep learning for melting heat transfer analysis with model-based transfer learning, *Computers & Mathematics with Applications*, 143, 2023, 303-317.
[39] Li, B., Guo, H., Zhuang, X., Material design with topology optimization based on the neural network, *International Journal of Computational Methods*, 19(08), 2022, 2142013.
[40] Padmanabha, G.A., Safta, C., Bouklas, N., Jones, R.E., Condensed Stein Variational Gradient Descent for Uncertainty Quantification of Neural Networks, *arXiv preprint*, 2024, arXiv: 2412.16462.
[41] Fuhg, J.N., Kalogeris, I., Fau, A., Bouklas, N., Interval and fuzzy physics-informed neural networks for uncertain fields, *Probabilistic Engineering Mechanics*, 68, 2022, 103240.
[42] Nasution, M.K., Syah, R., Ramdan, D., Afshari, H., Amirabadi, H., Selim, M.M., Khan, A., Rahman, M.L., Sarjadi, M.S., Su, C.H., Modeling and computational simulation for supersonic flutter prediction of polymer/GNP/fiber laminated composite joined conical-conical shells, *Arabian Journal of Chemistry*, 15(1), 2022, 103460.
[43] Affdl, J.H., Kardos, J., The Halpin-Tsai equations: a review, *Polymer Engineering & Science*, 16(5), 1976, 344-352.
[44] Keshtegar, B., Motezaker, M., Kolahchi, R., Trung, N.T., Wave propagation and vibration responses in porous smart nanocomposite sandwich beam resting on Kerr foundation considering structural damping, *Thin-Walled Structures*, 154, 2020, 106820.
[45] Gan, L.L., She, G.L., Nonlinear transient response of magneto-electro-elastic cylindrical shells with initial geometric imperfection, *Applied Mathematical Modelling*, 132, 2014, 166-186.
[46] Reddy, J., *Mechanics of laminated plates and shells theory and analysis*, CRC Press, Boca Raton, FL, 2004.
[47] Reddy, J., *Theory and Analysis of Elastic Plates and Shells*, 2nd Edition, CRC Press, 2006.
[48] Wolf, J., *Dynamic Soil/Structure Interaction*, Prentice Hall, Inc., Englewood Cliffs, New Jersey, 1985.
[49] Natarajan, S., Manickam, G., Bending and vibration of functionally graded material sandwich plates using an accurate theory, *Finite Elements in Analysis and Design*, 57, 2012, 32-42.
[50] Thai, C.H., Kulasegaram, S., Tran, L.V., Nguyen, X.H., Generalized shear deformation theory for functionally graded isotropic and sandwich plates based on isogeometric approach, *Computers & Structures*, 141, 2014, 94-112.
[51] Vasiraja N., Nagaraj P., The effect of material gradient on the static and dynamic response of layered functionally graded material plate using finite element method, *Bulletin of the Polish Academy of Sciences: Technical Sciences*, 2019, 827-838.
[52] Shahsavari, D., Shahsavari, M., Li, L., Karami, B., A novel quasi-3D hyperbolic theory for free vibration of FG plates with porosities resting on Winkler/Pasternak/Kerr foundation, *Aerospace Science and Technology*, 72, 2018, 134-149.
[53] Baferani, A.H., Saidi, A., Ehteshami, H., Accurate solution for free vibration analysis of functionally graded thick rectangular plates resting on elastic foundation, *Composite Structures*, 93(7), 2011, 1842-1853.
[54] Abuteir, B., Harkati, E., Boutagouga, D., Mamouri, S., Djeghaba, K., Thermo-mechanical nonlinear transient dynamic and Dynamic-Buckling analysis of functionally graded material shell structures using an implicit conservative/decaying time integration scheme, *Mechanics of Advanced Materials and Structures*, 29(27), 2022, 5773-5792.
[55] Tornabene, F., Bacciocchi, M., Fantuzzi, N., Reddy, J., Multiscale approach for three-phase CNT/polymer/fiber laminated nanocomposite structures, *Polymer Composites*, 40(S1), 2019, 102-126.

ORCID iD

Pham Binh Le https://orcid.org/0000-0003-2023-6275
Chung Pham https://orcid.org/0009-0001-6778-2057
Truong Thi Huong Huyen https://orcid.org/0000-0003-2189-3680
Nguyen Manh Dung https://orcid.org/0009-0001-8284-9985
Tran Trung Thanh https://orcid.org/0000-0002-1730-0590

How to cite this article: Le P.B., Pham C., Huong Huyen T.T., Dung N.M., Thanh T.T. Vibration characteristics-based isogeometric analysis of sandwich plates with an auxetic honeycomb core and laminated three-phase skin layers resting on Kerr foundation, *J. Appl. Comput. Mech.*, 11(4), 2025, 1087-1102. https://doi.org/10.22055/jacm.2025.48044.4937